Heat Transfer and Velocity Distribution in Liquid Metal Magneto-convective Flows Around Cooling Pipes

Chiara Mistrangelo, Leo Bühler, and Biao Lyu

***Abstract*—In the water-cooled lead lithium (WCLL) breeding blanket, the released thermal power is extracted by water-cooled pipes around which the PbLi circulates. The magnetohydrodynamic (MHD) flow that establishes in the blanket is determined mainly by the action of driving buoyancy forces, due to density gradients, and braking effects caused by viscosity and electromagnetic forces. The latter are induced by the interaction of the electrically conducting PbLi with the plasma-confining magnetic field. The characteristics of the magneto-convective flow depend on thermal conditions, such as differential or volumetric heating, geometry, electrical properties of the structural material, and reciprocal orientation of gravity and magnetic field. In the present study, we investigate numerically MHD-convective flows in closed geometries with differential heating and internal cylindrical obstacles that represent the cooling pipes, as present in the breeding zone of the WCLL blanket. The effects of applied temperature gradient, strength, and orientation of imposed magnetic field are studied via 3-D numerical simulations. The aim of the analysis is getting an overview of flow features and heat transfer properties depending on operating conditions and geometrical setups. It is found that the most intense convective flow occurs when the magnetic field is aligned with the cooling pipes since this configuration allows for quasi-2-D flow patterns with only moderate magnetic damping. The strongest reduction of convection is observed when the magnetic field is perpendicular to the pipes. In the latter case, the core velocity is significantly reduced, while the convective heat transport is confined to thin layers aligned with the magnetic field parallel to external walls or tangent to the pipes.**

***Index Terms*—Flow obstacles, heat transfer, liquid metal blankets, magnetohydrodynamics (MHD).**

I. Introduction

MAGNETO-convection in liquid metals results from the combined effects of thermal convection and electromagnetic forces that arise in electrically conducting fluids exposed to a magnetic field and in the presence of temperature gradients. These conditions are present in various technical and industrial applications, such as nuclear fusion reactors [1], crystal growth [2], and material processing [3]. Depending on magnetic field strength and its orientation with respect to gravity and temperature gradient, applying a magnetic field can lead to the suppression of turbulence and the inhibition of heat transfer or to the enhancement of convective motion via production of anisotropic turbulence or the occurrence of instabilities. Some examples may be found in the review article by Zikanov et al. [4] 2001. Numerical simulations and experiments are used to investigate established flow patterns, temperature distribution, and heat transfer in magneto-convective flows, with the aim of achieving a deeper understanding of such phenomena in order to optimize the design and performance of the process under study.

For applications in fusion reactor technology, different concepts for the breeding blanket are being developed. This component serves to produce tritium, one of the plasma fuel components, to extract the thermal power released by fusion neutrons, and to protect the magnets from radiation-induced damage. Among possible blanket designs, the water-cooled lead lithium (WCLL) breeding blanket has been selected to be tested during the experimental campaign carried out in the International Thermonuclear Experimental Reactor, ITER, and as a driver blanket concept for a EU-DEMO fusion reactor [5], [6]. In this blanket design, the lead lithium eutectic alloy, PbLi, is used as tritium breeder, neutron multiplier, and heat transfer medium. Volumetric heating in the liquid metal is produced by the high-energy neutrons that release their kinetic energy via nuclear reactions with the breeder material. In the breeding zones of the WCLL blanket, which consist of rectangular boxes delimited by first wall, backplate and radial–toroidal stiffening plates, the thermal power is extracted by water-cooled pipes around which the PbLi circulates. In Fig. 1, a radial–toroidal cut and a 3-D view show the main structure of the WCLL blanket. Due to the presence of the intense plasma-confining magnetic field, flow-induced electric currents generate electromagnetic Lorentz forces that significantly affect the flow structure and its heat transfer properties. In the WCLL blanket concept, the forced flow of the liquid metal is weak and it is required to transport the PbLi toward external facilities for tritium extraction and purification. As a result of this small velocity, the magnetohydrodynamic (MHD) pressure drop that arises from the occurrence of the Lorentz forces does not represent a critical feasibility issue for this blanket design [7]. However, the presence of cooling pipes,

Received 30 September 2025; revised 2 March 2026; accepted 27 April 2026. This work was supported by the EUROfusion Consortium funded by European Union through the Euratom Research and Training Program under Grant 101052200. The review of this article was arranged by Senior Editor M. Kovari. *(Corresponding author: Chiara Mistrangelo.)*

The authors are with Karlsruhe Institute of Technology, 76021 Karlsruhe, Germany (e-mail: chiara.mistrangelo@kit.edu; leo.buehler@kit.edu; biao.lyu@kit.edu).

Color versions of one or more figures in this article are available at https://doi.org/10.1109/TPS.2026.3691446

Digital Object Identifier 10.1109/TPS.2026.3691446

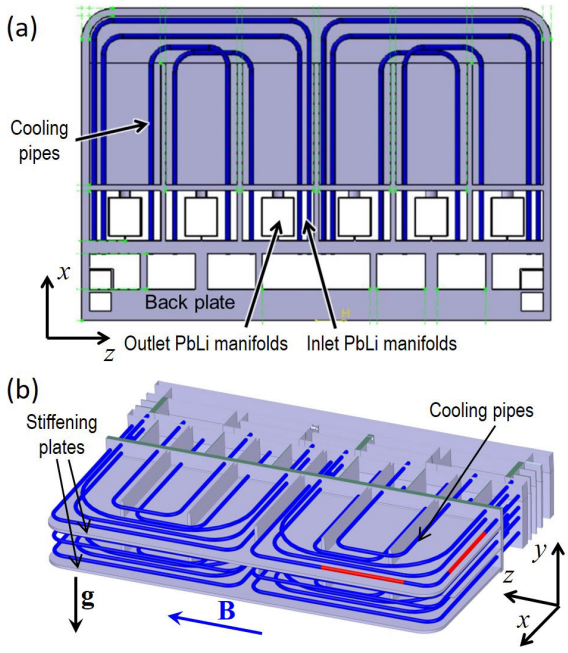

Fig. 1. WCLL blanket design. (a) Radial–toroidal and (b) 3-D views on breeding zones, manifolds, and cooling pipes. The two red portions of the cooling pipes in (b) indicate geometrical setups that explain the cases selected for the present study.

which partially block the flow and generate large thermal gradients within the fluid, results in complex convective flow patterns that influence heat and mass transfer in the breeder units. Features of the flow and effects of electromagnetic braking depend on the orientation of the magnetic field with respect to gravity and applied thermal gradients.

While magnetoconvection in pipes and channels has been extensively investigated both theoretically and experimentally (see [4]), heat transfer and flow distribution around obstacles immersed in liquid metal did not receive the same attention. Few numerical [8], [9] and experimental works [10] can be found in the literature dealing with this problem and the possible consequences for applications in fusion technology. In the past, focus was placed on fundamental convective flows such as the Rayleigh–Bénard problem [11], [12], [13], where a horizontal fluid layer is heated from below or differentially heated cavities with a given temperature gradient [14], [15], [16], where a uniform magnetic field is imposed.

In the present article, we summarize the results from the study of magneto-convective flow in an adiabatic and thermally insulating rectangular box filled with gallium–indium–tin. Temperature gradients, driving the convective motion, originate from the presence of two horizontal parallel pipes immersed in the liquid metal and kept at constant differential temperatures. This geometrical setup and the model fluid GaInSn have been used for experiments in the MEKKA laboratory at KIT [10] in a uniform magnetic field, $\mathbf{B} = B_y\hat{\mathbf{y}}$, applied parallel to gravity and perpendicular to the axis of the pipes (see Section II). Magneto-convective flows in this configuration have been investigated both numerically and experimentally in previous studies [9], [10]. As visible in Fig. 1(b), the above described

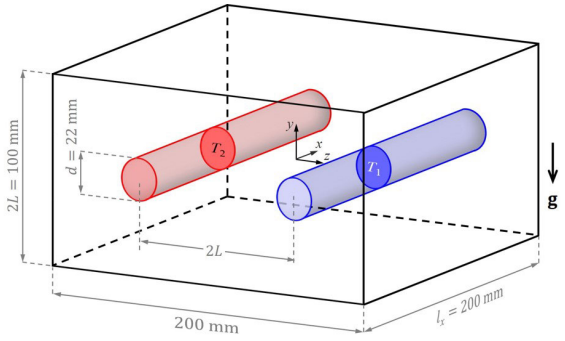

Fig. 2. Model geometry used for the simulations and reproducing the experimental test section. The direction of the magnetic field is not indicated, since it is used as a parameter in the present study.

arrangement of magnetic field, gravity, and thermal gradient is not strictly related to the WCLL blanket design, but it can be regarded as a fundamental study of MHD convection and was selected due to the experimental constraints. For that reason, additional simulations have been performed for two complementary cases in which the magnetic field is perpendicular to gravity. In the first configuration, the axis of the tubes is aligned with the magnetic field, while in the second one, it is perpendicular. The former corresponds to cooling pipes aligned with the first wall, and the latter corresponds to those in the radial direction. In Fig. 1(b), red portions of pipes highlight the corresponding situations in the present WCLL blanket design.

II. Problem Definition and Model Geometry

The liquid metal magneto-convective flow in an adiabatic and electrically insulating rectangular cavity is investigated numerically. Two electrically insulating parallel cylinders are inserted horizontally in the box, aligned with the x coordinate, as shown in Fig. 2. The typical length L of the geometry corresponds to half the distance between top (y_{max}) and bottom (y_{min}) walls. This choice is related to the experimental setup, as described in [10] and [17], where the magnetic field is parallel to the y coordinate. For the description of the results, we will refer to the walls located at $x = x_{min}, x_{max}$ as end-walls. In the coordinate system centered in the middle of the cavity, the axes of the two pipes are positioned at $z = \pm L = \pm 0.05$m, i.e., L is also a characteristic scale for the distance between the cylinders, which is related to the horizontal temperature gradient that drives the convective motion in the fluid. In this configuration, the pipes are kept at constant temperatures, $T_1 = T_0 - \Delta T$ and $T_2 = T_0 + \Delta T$, where T_0 is the mean temperature.

III. Mathematical Model and Flow Parameters

The buoyancy-driven MHD flow investigated in the present study can be mathematically described by Navier–Stokes equations that account for conservation of momentum and mass, in which buoyancy and electromagnetic forces appear as source terms. Electric currents used to calculate the Lorentz force are determined via Ohm's law

$$\rho_0\left(\frac{\partial}{\partial t}+\mathbf{u}\cdot\nabla\right)\mathbf{u} = -\nabla p+\rho_0\nu\nabla^2\mathbf{u} + \mathbf{j}\times\mathbf{B}-\rho_0\beta(T-T_0)\,\mathbf{g} \qquad (1)$$

TABLE I

MATERIAL PROPERTIES OF GaInSn AT T_0 [18]

T_0	ρ_0	$\nu \cdot 10^7$	$\sigma \cdot 10^{-6}$	$\beta \cdot 10^4$	k	c_p
°C	$\frac{\text{kg}}{\text{m}^3}$	$\frac{\text{m}^2}{\text{s}}$	$\frac{1}{\Omega\text{m}}$	$\frac{1}{\text{K}}$	$\frac{\text{W}}{\text{mK}}$	$\frac{\text{m}^2}{\text{s}^2\text{K}}$
30	6344.9	3.228	3.222	1.223	24.61	345.13

$$\nabla \cdot \mathbf{u} = 0, \quad \mathbf{j} = \sigma(-\nabla\phi + \mathbf{u} \times \mathbf{B}). \tag{2}$$

According to the Boussinesq approximation, density variations $\rho(T)$ appear only in the buoyancy term in (1), where ρ_0 is the density taken at the reference temperature T_0. The variables u, p, j, B, T, and ϕ in (1) and (2) indicate velocity, pressure, current density, applied magnetic flux density, temperature, and electric potential. The temperature distribution is calculated by solving an energy balance equation

$$\rho_0 c_p \left(\frac{\partial T}{\partial t} + \mathbf{u} \cdot \nabla T \right) = \nabla \cdot (k \nabla T). \tag{3}$$

The thermophysical properties of the fluid, i.e., reference density ρ_0, viscosity ν, coefficient of volumetric thermal expansion β, electrical and thermal conductivities σ and k, and the specific heat capacity c_p, are taken at the mean temperature T_0 according to [18] and summarized in Table I.

It is assumed that the flow is inductionless, i.e., the magnetic field is stationary and not affected by the flow. This assumption is usually valid when the magnetic Reynolds number $R_m = \mu\sigma u_0 L$ is small, as in the discussed case. Here, μ stands for the magnetic permeability and u_0 is the characteristic velocity in the problem. The relevant nondimensional parameters for buoyant MHD flow are the Hartmann number Ha and the Grashof number Gr

$$Ha = BL\sqrt{\frac{\sigma}{\rho_0 \nu}}, \quad Gr = \frac{g\beta\Delta T L^3}{\nu^2}. \tag{4}$$

The square of the former quantifies the ratio of electromagnetic to viscous forces, while the latter denotes the relative importance of buoyant and viscous forces. For free convective flow in a magnetic field, the characteristic magnitude of velocity results from the balance of buoyant and electromagnetic forces and can be expressed as $u_0 = \rho\beta g\Delta T/\sigma B^2$, as outlined, e.g., in [19]. With this definition, it follows that the Reynolds number $Re = u_0 L/\nu$ is equivalent to the ratio Gr/Ha^2, and the square of the Lykoudis number $Ly^2 = Ha^4/Gr$ corresponds to the interaction parameter that represents the ratio of electromagnetic and inertia force.

IV. NUMERICAL RESULTS

Numerical simulations have been performed by using the finite volume open source code OpenFOAM. An in-house-developed segregated solver is employed where the Lorentz force is treated explicitly and defined at cell centers. The implementation of (1)–(3) in the code used in this study is based on a conservative algorithm, which uses the identity $\mathbf{j} = \nabla \cdot (\mathbf{jr})$, where r is the distance vector [20], [21], for calculating electric currents by interpolating face fluxes. This formulation minimizes nonphysical contributions to the Lorentz force arising from discretization errors. A thorough validation of the solver has been carried out by comparing results against both analytical solutions and experimental data. When studying numerically MHD flows, the accuracy of the solution depends significantly on the proper resolution of boundary layers whose thickness reduces with increasing the strength of the imposed magnetic field. According to the analysis of fully developed MHD flows in square channels, the accurate prediction of velocity, current distribution, and pressure gradient in a channel needs at least 7 grid points in Hartmann layers along walls perpendicular to the magnetic field and 20 nodes in parallel layers at walls aligned with B [22].

TABLE II

CASES INVESTIGATED IN THE PRESENT ANALYSIS. ORIENTATION OF B WITH RESPECT TO g AND TO THE PIPE AXIS

	B	Orientation of B with respect to g	Orientation of B with respect to pipe axis	Common features
Case 1	B_x	$\perp$	$\parallel$	g$\parallel$to $\hat{\mathbf{y}}$
Case 2	B_z	$\perp$	$\perp$	
Case 3	B_y	$\parallel$	$\perp$	ΔT $\parallel$to $\hat{\mathbf{z}}$

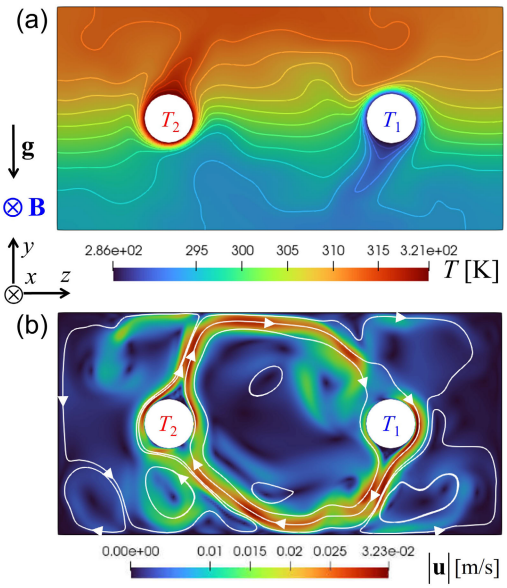

Fig. 3. *Case 1*: flow at $Ha = 500$, $Gr = 2.5 \times 10^7$ and $\mathbf{B} = B_x\hat{\mathbf{x}}$. Contours of (a) temperature and (b) velocity magnitude on the yz plane in the middle of the container. In (b), white curves are velocity streamlines.

In the following, we consider three cases of MHD-convective flow at constant parameters $Ha = 500$ and $Gr = 2.5 \cdot 10^7$, where we choose the orientation of the magnetic field parallel to the pipe axes along the x-coordinate (*Case 1*), aligned with the applied mean temperature gradient $\Delta T/\Delta z$ (*Case 2*), and parallel to gravity $\mathbf{g} = -g\hat{\mathbf{y}}$ (*Case 3*). The three arrangements are summarized in Table II. In *Cases 1* and *2*, the magnetic field is horizontal ($\perp$ to g). *Case 3* corresponds to the experimental setup as described in [17].

When the magnetic field is oriented along the axial direction as in *Case 1*, i.e., $\mathbf{B} = B_x\hat{\mathbf{x}}$, the temperature field is character-

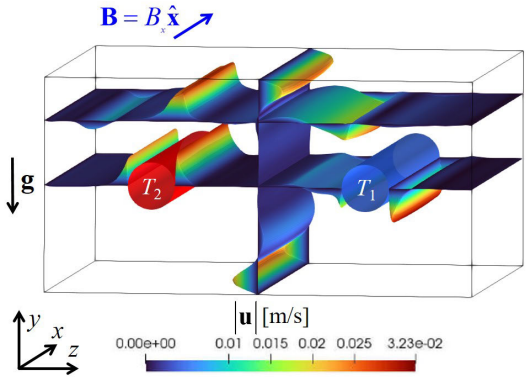

Fig. 4. *Case 1*: flow at $Ha = 500$, $Gr = 2.5 \times 10^7$ and $\mathbf{B} = B_x\hat{\mathbf{x}}$. Contours of velocity magnitude on different planes.

ized by thermal stratification in which the isotherms, especially in the central part of the box, are mainly horizontal as visible in Fig. 3(a). Here, contours of temperature are plotted on the yz plane in the middle of the box. This is an indication of a significant convective motion, as confirmed by velocity contours and streamlines depicted in Fig. 3(b). This magneto-convective flow features a high-velocity jet that creates a main large circulation between the tubes, which splits around the pipes and reunites behind the obstacles. Some fractions of the flow in the external boundary layers that form around the cylinders feed recirculations that redistribute the fluid in the outer lateral regions of the box. Other weaker structures are present above and below the pipes. In the center of the box, the velocity is almost negligible as well as close to the lateral side walls at $z = z_{min}, z_{max}$. This type of configuration allows for quasi-2-D flow patterns in yz planes with almost no variation along x, and there is only a weak magnetic damping. Only near the end-walls at $x = x_{min}, x_{max}$, in the thin Hartmann boundary layers perpendicular to the magnetic field, deviations from the 2-D behavior are observed. The established intense convective motion is characterized by time-dependent structures that lead to noticeable flow mixing.

A 3-D view of the flow distribution in the container is shown in Fig. 4, where contours of velocity are plotted on three planes. On the horizontal xz midplane, jets are visible in the tangential boundary layers along the pipes, which recombine behind the cylinders. The occurrence of recirculations is indicated by the presence of reversed flow on a single plane.

We consider now *Case 2*, in which the magnetic field, $\mathbf{B} = B_z\hat{\mathbf{z}}$, is horizontal and perpendicular to the axis of the pipes. In Fig. 5(a), 3-D contours of the velocity are plotted on six planes. We observe a completely different flow behavior compared to *Case 1*. The highest velocities are now confined in the boundary layers that develop along walls aligned with the magnetic field, i.e., top, bottom, and end-walls. The thickness of these parallel layers scales typically as $Ha^{-0.5}$. In the rest of the box, the velocity is very small. The main convective motion transports the fluid in y- and z-directions. However, a weak secondary flow is also present, superimposed on the main circulation. It carries the liquid metal in the x-direction toward the center of the box. This secondary recirculation is visualized by means of 2-D streamlines on the middle xy plane

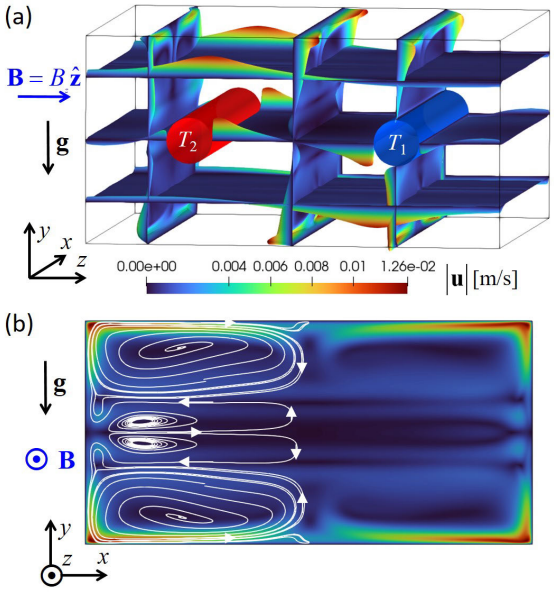

Fig. 5. *Case 2*: flow at $Ha = 500$ and $Gr = 2.5 \cdot 10^7$ and $\mathbf{B} = B_z\hat{\mathbf{z}}$. (a) Velocity distribution on different planes and (b) contours of velocity magnitude and 2-D streamlines of the secondary flow (shown only for $x < 0$) on the xy plane in the middle of the container. In the used representation, the distance between streamlines is not an indication of the velocity magnitude.

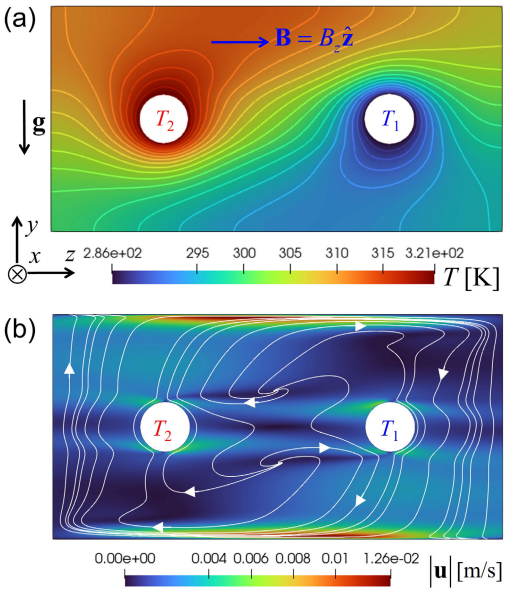

Fig. 6. *Case 2*: flow at $Ha = 500$ and $Gr = 2.5 \times 10^7$ and $\mathbf{B} = B_z\hat{\mathbf{z}}$. (a) Contours of temperature and (b) contours of velocity magnitude and streamlines on the yz plane in the middle of the container.

for $x < 0$ in Fig. 5(b). It should be mentioned that in the used representation, the distance between streamlines is not an indication of the velocity magnitude. The secondary flow is organized in three subregions almost separated from each other by internal horizontal layers that develop along magnetic field lines tangent to the pipes, known as Ludford layers [23], [24].

A first comparison between Figs. 3 and 6 suggests for this second setup an increased magnetic braking compared

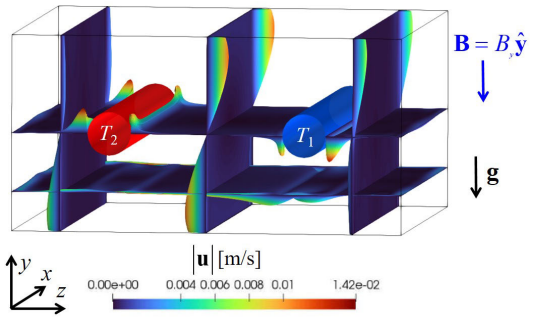

Fig. 7. *Case 3*: flow at $Ha = 500$, $Gr = 2.5 \times 10^7$ and $\mathbf{B} = B_y\hat{\mathbf{y}}$. Contours of velocity on different planes.

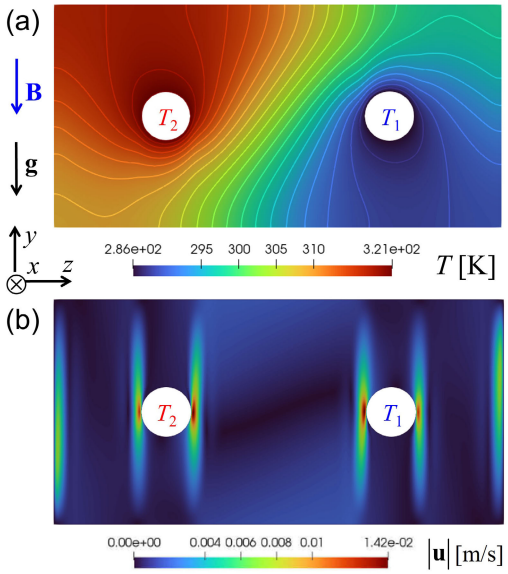

Fig. 8. *Case 3*: flow at $Ha = 500$, $Gr = 2.5 \times 10^7$, and $\mathbf{B} = B_y\hat{\mathbf{y}}$. Contours of (a) temperature and (b) velocity magnitude plotted on the yz plane in the middle of the box.

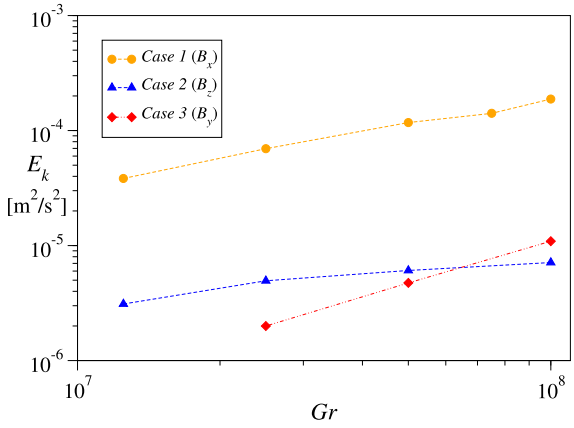

Fig. 9. Average kinetic energy E_k for $Ha = 500$, three orientations of the magnetic field and different Grashof numbers Gr.

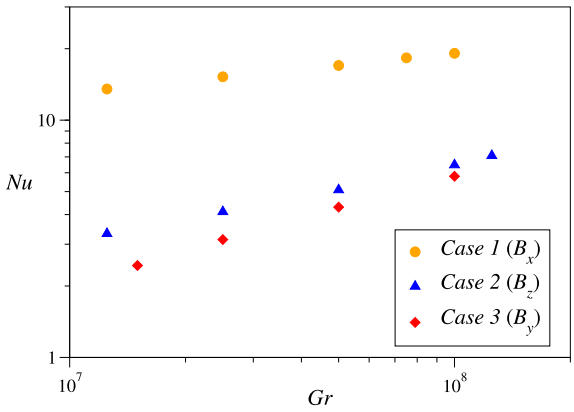

Fig. 10. Nusselt number Nu as a function of the Grashof number Gr for the three cases analyzed in the study and $Ha = 500$.

to the previous one. This stronger electromagnetic damping stabilizes the flow that becomes laminar and stationary with reduced velocity in the core and jets in the parallel layers. A deviation of the temperature distribution from the previously observed thermal stratification [see Fig. 3(a)] reveals as well a reduced convective transport compared to *Case 1*.

The last setup, *Case 3*, has already been discussed in detail in a previous publication, where a comparison with experimental data has been presented as well [9]. For completeness of the present study, we summarize here the main features of this type of flow for the given parameters.

Fig. 7 shows the contours of velocity on different planes in the box. Along all walls parallel to the magnetic field, boundary layers form with higher velocity in the form of confined jets. Ludford layers develop in the vertical direction aligned with the magnetic field and tangential to the two pipes. These layers are clearly visible in Fig. 8(b), where contours of velocity magnitude are plotted on a yz plane in the middle of the box. While Ludford layers in *Case 2* act primarily as separators between distinct flow cores, in the present *Case 3*, they carry in addition some fraction of flow.

The highest values of the velocity are localized in the parallel layers along the end-walls at $x = x_{min}, x_{max}$. The convective flow is characterized by large circulations, in particular the one between the two pipes, that exchange the fluid among internal and boundary parallel layers. The velocity in the cores, outside the internal and side layers, is very small, even negligible. The temperature distribution visualized in Fig. 8(a) on the middle plane indicates that there is a certain contribution of convective flow since the isotherms are still inclined with respect to gravity, even if it is weaker compared to previous cases. However, conduction becomes more important. This stems from the significant role of the magnetic damping exerted by the induced electromagnetic Lorentz forces on the flow. By increasing further the magnetic field (Ha) or reducing the imposed temperature gradient (Gr), the relative importance of buoyancy forces compared to the electromagnetic ones decreases and the isotherms tend to become more vertical [9], [10].

All previous observations are supported by considering the average kinetic energy in the volume V of the box as a measure for the intensity of the convective flow

$$E_k = \frac{1}{V}\int_V \mathbf{u}^2 dV.$$

Values of E_k are plotted as a function of the Grashof number Gr in Fig. 9 for the three cases discussed in the article. The data clearly show how the orientation of the magnetic field determines the strength of the electromagnetic damping on flow structures and, accordingly, the intensity of the convective motion in the container and confirm previous observations.

The intensity of the convective heat transfer between pipes and liquid metal can be quantified by the dimensionless Nusselt number Nu defined as

$$Nu = \frac{hL}{k} \tag{5}$$

where the heat transfer coefficient h determines the average surface heat flux on the pipes, i.e., $\overline{q} = h\Delta T$. The variation of the Nusselt number, evaluated at the cylinder walls, as a function of the Grashof number is shown in Fig. 5 for the three cases investigated (see Table II). An increase in the Nusselt number indicates that the convective heat transfer becomes more significant compared to the purely conductive one. The data clearly show that *Case 1* leads to the strongest convective heat transport.

Few preliminary simulations have been carried out for an additional Hartmann number ($Ha = 250$) and some Grashof numbers, in order to gain an initial understanding of how the strength of the magnetic field influences the flow. It can be observed that in *Case 1*, a quasi-2-D flow featuring recirculations with axes aligned with the magnetic field is already established even for the smaller Ha. For horizontal and vertical transverse magnetic fields, i.e., for *Cases 2* and *3*, the tangent layers become thicker and a more significant influence of inertia effects in these layers can be noticed when $Ha = 250$. For all the analyzed cases, by decreasing the Hartmann number, the strength of the convective motion increases due to the reduced damping exerted by the weaker electromagnetic forces. As a result, Nu increases when Ha is smaller.

V. Conclusion

Numerical simulations have been carried out to investigate the magneto-convective flow in a liquid metal-filled cavity, in which two parallel pipes are inserted and kept at constant differential temperatures. The magnitude of the convective motion depends on the reciprocal orientation of magnetic field, gravity, and temperature gradient. The intensity of the differential heating, quantified by the Grashof number Gr, determines the mixing of the flow and the strength of the convective motion. The imposed magnetic field, expressed by the Hartmann number Ha controls the braking of the fluid motion by electromagnetic forces. The parameters used in the current analysis have been chosen in a range that can be reached by laboratory experiments, i.e., Ha is at least one order of magnitude smaller than in WCLL blankets, and Gr, based here on the temperature difference ΔT, should be rewritten in terms of volumetric heating for nuclear fusion applications.

Three different cases have been analyzed by choosing the magnetic field along the x (*Case 1*), z (*Case 2*), and y (*Case 3*) coordinates. The orientation of the magnetic field completely changes the structure of the flow and the way in which the liquid metal circulates around the obstacles. With same characteristic parameters (Ha and Gr), the strongest convective heat transfer occurs when B is aligned with the cooling pipes (*Case 1*, $\mathbf{B} = B_x\hat{\mathbf{x}}$). This orientation of the magnetic field along the pipe axes is met in WCLL blankets close to the plasma-facing first wall, as sketched in Fig. 1(b). By turning the magnetic field in a horizontal direction perpendicular to the pipes, as in the case of water pipes with radial orientation in the WCLL blanket breeding zone (*Case 2*, $\mathbf{B} = B_z\hat{\mathbf{z}}$), the magnetic damping increases. The strongest braking is observed when B is vertical (*Case 3*, $\mathbf{B} = B_y\hat{\mathbf{y}}$). The latter setup would correspond to a purely poloidal magnetic field, which is not found in WCLL blankets. However, this arrangement has been considered since it conforms to experimental constraints in the MEKKA laboratory at KIT, where related experiments have been performed.

An ongoing parametric study aims at complementing the present data and supporting the derivation of a heat transfer correlation for the Nusselt number in the form $Nu(Gr, Ha, \mathbf{B}\text{-orientation})$.

Acknowledgment

Views and opinions expressed are, however, those of the author(s) only and do not necessarily reflect those of the European Union or European Commission. Neither the European Union nor the European Commission can be held responsible for them.

References

[1] C. Mistrangelo, L. Bühler, S. Smolentsev, V. Klüber, I. Maione, and J. Aubert, "MHD flow in liquid metal blankets: Major design issues, MHD guidelines and numerical analysis," *Fusion Eng. Design*, vol. 173, Dec. 2021, Art. no. 112795.

[2] V. Galindo, G. Gerbeth, W. von Ammon, E. Tomzig, and J. Virbulis, "Crystal growth melt flow control by means of magnetic fields," *Energy Convers. Manage.*, vol. 43, no. 3, pp. 309–316, Feb. 2002.

[3] H. Yasuda, "Applications of high magnetic fields in materials processing," in *Magnetohydrodynamics*, vol. 80. Dordrecht, The Netherlands: Springer, 2007, pp. 329–344.

[4] O. Zikanov, I. Belyaev, Y. Listratov, P. Frick, N. Razuvanov, and V. Sviridov, "Mixed convection in pipe and duct flows with strong magnetic fields," *Appl. Mech. Rev.*, vol. 73, no. 1, pp. 1–010801, Jan. 2021.

[5] G. Federici, L. Boccaccini, F. Cismondi, M. Gasparotto, Y. Poitevin, and I. Ricapito, "An overview of the EU breeding blanket design strategy as an integral part of the DEMO design effort," *Fusion Eng. Design*, vol. 141, pp. 30–42, Apr. 2019.

[6] P. Arena et al., "Design and integration of the EU-DEMO water-cooled lead lithium breeding blanket," *Energies*, vol. 16, no. 4, p. 2069, Feb. 2023.

[7] S. Smolentsev, "Physical background, computations and practical issues of the magnetohydrodynamic pressure drop in a fusion liquid metal blanket," *Fluids*, vol. 6, no. 3, p. 110, Mar. 2021.

[8] A. Tassone, G. Caruso, F. Giannetti, and A. Del Nevo, "MHD mixed convection flow in the WCLL: Heat transfer analysis and cooling system optimization," *Fusion Eng. Design*, vol. 146, pp. 809–813, Sep. 2019.

[9] C. Mistrangelo, L. Bühler, H.-J. Brinkmann, C. Courtessole, V. Klüber, and C. Koehly, "Magneto-convective flows around two differentially heated cylinders," *Heat Mass Transf.*, vol. 59, no. 11, pp. 2005–2021, Nov. 2023.

[10] C. Courtessole, H.-J. Brinkmann, and L. Bühler, "Experimental investigation on magneto-convective flows around two differentially heated horizontal cylinders," *J. Fluid Mech.*, vol. 993, pp. A6–1–A6–22, Aug. 2024.

[11] R. M. Clever and F. H. Busse, "Nonlinear oscillatory convection in the presence of a vertical magnetic field," *J. Fluid Mech.*, vol. 201, pp. 507–523, Apr. 1989.

[12] T. Zürner, F. Schindler, T. Vogt, S. Eckert, and J. Schumacher, "Flow regimes of Rayleigh–Bénard convection in a vertical magnetic field," *J. Fluid Mech.*, vol. 894, p. A21, Jul. 2020.
[13] J. H. P. Dawes, "Localized convection cells in the presence of a vertical magnetic field," *J. Fluid Mech.*, vol. 570, pp. 385–406, Jan. 2007.
[14] J. P. Garandet, T. Alboussiere, and R. Moreau, "Buoyancy driven convection in a rectangular enclosure with a transverse magnetic field," *Int. J. Heat Mass Transf.*, vol. 35, no. 4, pp. 741–748, Apr. 1992.
[15] S. Aleksandrova and S. Molokov, "Three-dimensional buoyant convection in a rectangular cavity with differentially heated walls in a strong magnetic field," *Fluid Dyn. Res.*, vol. 35, no. 1, pp. 37–66, Jul. 2004.
[16] L. Chen, B.-Q. Liu, and M.-J. Ni, "Study of natural convection in a heated cavity with magnetic fields normal to the main circulation," *Int. J. Heat Mass Transf.*, vol. 127, pp. 267–277, Dec. 2018.
[17] C. Koehly, L. Bühler, and C. Mistrangelo, "Design of a test section to analyze magneto-convection effects in WCLL blankets," *Fusion Sci. Technol.*, vol. 75, no. 8, pp. 1010–1015, Nov. 2019.
[18] Y. Plevachuk, V. Sklyarchuk, S. Eckert, G. Gerbeth, and R. Novaković, "Thermophysical properties of the liquid Ga–In–Sn Eutectic alloy," *J. Chem. Eng. Data*, vol. 59, no. 3, pp. 757–763, 2014.
[19] L. N. Hjellming and J. S. Walker, "Melt motion in a Czochralski crystal puller with an axial magnetic field: Motion due to buoyancy and thermocapillarity," *J. Fluid Mech.*, vol. 182, pp. 335–368, Sep. 1987.
[20] M.-J. Ni, R. Munipalli, N. B. Morley, P. Huang, and M. A. Abdou, "A current density conservative scheme for incompressible MHD flows at a low magnetic Reynolds number. Part I: On a rectangular collocated grid system," *J. Comput. Phys.*, vol. 227, no. 1, pp. 174–204, Nov. 2007.
[21] M.-J. Ni, R. Munipalli, P. Huang, N. B. Morley, and M. A. Abdou, "A current density conservative scheme for incompressible MHD flows at a low magnetic Reynolds number. Part II: On an arbitrary collocated mesh," *J. Comput. Phys.*, vol. 227, no. 1, pp. 205–228, Nov. 2007.
[22] S. Smolentsev et al., "An approach to verification and validation of MHD codes for fusion applications," *Fusion Eng. Design*, vol. 100, pp. 65–72, Nov. 2015.
[23] G. S. S. Ludford, "Inviscid flow past a body at low magnetic Reynolds number," *Rev. Modern Phys.*, vol. 32, no. 4, pp. 1000–1003, Oct. 1960.
[24] J. C. R. Hunt and S. Leibovich, "Magnetohydrodynamic flow in channels of variable cross-section with strong transverse magnetic fields," *J. Fluid Mech.*, vol. 28, no. 2, pp. 241–260, May 1967.

Chiara Mistrangelo received the Ph.D. degree in fluid dynamics from Karlsruhe University, Karlsruhe, Germany, in 2005.

She is a Senior Researcher and a Lecturer at the Department for Thermal Energy Technology and Safety, KIT. Her current research interests include pressure- and buoyancy-driven convective MHD flows in complex geometries, code development, validation through experiments, and benchmark activities.

Leo Bühler received the Dr.-Ing. degree and the Habilitation degree in fluid dynamics from Karlsruhe University, Karlsruhe, Germany, in 1992 and 2008, respectively.

He is a Professor at the Department for Thermal Energy Technology and Safety, KIT, and the Head of the MHD Research Group with MEKKA and MaPLE facilities. His research interests include any kind of MHD flow in generic and complex geometries, asymptotic analysis, code development, and validation through experiments.

Biao Lyu, photograph and biography not available at the time of publication.